Supporting Information

Szundi et al. 10.1073/pnas.1008603107

SI Text

Kinetic Analysis. A brief summary of the algebraic method of kinetic analysis is given below. The time-dependence of the optical absorption matrix **A** (λ, *t*), recorded for pseudo-first-order reactions, can be represented by a sum of exponential functions:

$$\mathbf{A}(\lambda,t) = \Sigma b_i(\lambda)\exp(-r_i t),$$

where $b_i(\lambda)$ are the amplitudes at each wavelength, the so-called *b*-spectra, and r_i are the apparent rate constants, the inverse of the lifetimes, $\tau_i(r_i = 1/\tau_i)$. The global exponential fitting is carried out using singular value decomposition (SVD). In the SVD analysis, the data matrix, **A** (λ,t), is presented as the product of three matrices **U**, **S**, and **V**,

$$\mathbf{A} = \mathbf{USV}',$$

which represent the orthonormal basis spectra (**u**-spectra), the corresponding singular values, and the **v**-vectors describing time-evolution of the corresponding **u**-spectra. Keeping only the significant, **U**, **S** and **V** vectors, the SVD analysis reduces noise and significantly decreases the number of time-dependent traces subject to the exponential fitting. SVD also provides a good estimate of the minimum number of spectrally distinct intermediates present. The *b*-spectra and the apparent rates are directly related to the underlying physical mechanism or scheme, which contains the microscopic rates, the actual rates of the reaction steps. In the algebraic method of the kinetic analysis, the microscopic rates are arranged in a kinetic matrix, **K**, the eigenvalues of which give the apparent rates. Its eigenvectors, $\mathbf{w}_i$ are related to the *b*-spectra through

$$b_i(\lambda) = \mathbf{E} \times \mathbf{w}_i,$$

where **E** is the matrix of intermediate spectra. The apparent rates and *b*-spectra, obtained from the experimental absorbance matrix $\mathbf{A}(\lambda,t)$, form the basis for proposing the kinetic scheme. The validity of the scheme is judged by the intermediate spectra, **E**, it produces:

$$\mathbf{E} = b \times \mathbf{w}^{-1}.$$

In many cases, expectations regarding the shapes and amplitudes of the intermediate spectra can be clearly defined.

Analysis of a Reversible O_2-Binding Scheme. The following analysis pertains to testing the plausibility of the five-step mechanism of the reduction of dioxygen to water by ba_3 (in the absence of CO) in which the O_2 binding is reversible (Scheme S1).

The first step in the description of this scheme is the construction of the kinetic matrix, **K**, containing the microscopic rates in the reversible scheme:

$$\mathbf{K} = \begin{pmatrix} -k_{12} & k_{21} & 0 & 0 & 0 \\ k_{12} & -(k_{21}+k_{23}) & 0 & 0 & 0 \\ 0 & k_{23} & -k_{34} & 0 & 0 \\ 0 & 0 & k_{34} & -k_{45} & 0 \\ 0 & 0 & 0 & k_{45} & 0 \end{pmatrix}.$$

The eigenvalues λ_i of **K** can be obtained from the determinant, $\det(\mathbf{K}\text{-}\lambda\mathbf{I}) = 0$, where **I** is the identity matrix:

$$\lambda(\lambda+k_{45})(\lambda+k_{34})[(\lambda+k_{12})(\lambda+k_{21}+k_{23}) - k_{12}k_{21}] = 0. \quad \textbf{[S1]}$$

The eigenvalues of the kinetic matrix with the sign reversed are the apparent rates, namely,

$$r_i = -\lambda_i. \quad \textbf{[S2]}$$

Two of the apparent rates are equal to the microscopic rates of the last two steps:

$$r_3 = k_{34} \qquad r_4 = k_{45}. \quad \textbf{[S3]}$$

Solving the quadratic equation,

$$\lambda^2 + (k_{12}+k_{21}+k_{23})\lambda + k_{12}k_{23} = 0, \quad \textbf{[S4]}$$

provides two more apparent rates, r_1 and r_2. Instead of solving the quadratic equation, we make use of the general formulas that relate the roots of a quadratic equation to the coefficients and the free term:

$$r_1 + r_2 = (k_{12}+k_{21}+k_{23}) \qquad r_1 r_2 = k_{12}k_{23}. \quad \textbf{[S5]}$$

By introducing the equilibrium constant $Q = k_{12}/k_{21}$ as a variable, we can obtain k_{23}, k_{12} and k_{21} as a function of Q:

$$k_{23} = \{r_1 + r_2 \pm [(r_1+r_2)^2 - 4r_1r_2(1+1/Q)]^{1/2}\}/2, \quad \textbf{[S6]}$$

$$k_{12} = r_1 r_2 / k_{23}, \quad \textbf{[S7]}$$

$$k_{21} = r_1 r_2 / k_{23} Q. \quad \textbf{[S8]}$$

Considering only real number solutions for k_{23} requires the discriminant in Eq. **S6** to be nonnegative, which places the following limits on Q:

$$Q \geq 4r_1r_2/(r_1 - r_2)^2.$$

Consequently, $Q_{\min}$, the lower limit of Q is:

$$Q_{\min} = 4r_1r_2/(r_1-r_2)^2 = 4\tau_1\tau_2/(\tau_2-\tau_1)^2. \quad \textbf{[S9]}$$

For $Q_{\min}$, the microscopic rates are:

$$k_{23} = (\tau_1+\tau_2)/2\tau_1\tau_2; \qquad k_{12} = 2/(\tau_1+\tau_2);$$
$$k_{21} = (\tau_2-\tau_1)^2/2(\tau_1+\tau_2)\tau_1\tau_2.$$

For any $Q > Q_{\min}$, the microscopic rates, k_{12}, k_{21}, and k_{23}, are functions of Q and can be obtained using Eqs. **S6**, **S7**, and **S8** shown above. It should be noted that there are two sets of *k* values for any $Q > Q_{\min}$. At $Q = \infty$, k_{12} and k_{23} can each approach the values of both r_1 and r_2. When $k_{12} = r_1$ and $k_{23} = r_2$, we have the traditional fast-to-slow order of microscopic rates. However, when $k_{12} = r_2$ and $k_{23} = r_1$, we have a slow-fast rate combination for the first two steps, a rather unorthodox way of arranging the experimental apparent rates of the first two steps in a kinetic scheme.

As mentioned above, at any $Q > Q_{\min}$ all three microscopic rates have two values (Eqs. **S6**, **S7**, and **S8**). To test the mechanism, the microscopic rate constants, k_{12}, k_{21}, and k_{23}, in Scheme S1

are deduced from the first two apparent lifetimes at a set of Q values and the most plausible sets of rates selected based on the best agreement between the calculated spectrum of Int 2 (compound **A**) and that of the model spectrum; when modeling the O_2 binding in ba_3, the spectrum of compound **A** of the bovine enzyme, obtained in a conventional CO flow-flash experiment at high O_2 concentration, serves as the model spectrum. As discused above, the spectrum of Int 2 is calculated at three Q values from the b-spectra and the eigenvectors of the corresponding kinetic matrix containing the set of microscopic rates.

The relationship between the microscopic rates and apparent rates shown above indicates that the interpretation of kinetics involving a reversible step is not always trivial. According to "traditional" interpretation, the equilibrium of the first step is going to be established with an apparent rate of $(k_{12} + k_{21})$. Similarly, the apparent rate of the irreversible step following the equilibrium step is expected to "slow down" according to the formula $k_{23}k_{12}/(k_{12} + k_{21})$, which is commonly interpreted as arising from a lower concentration of intermediate 2 in the equilibrium mixture. However, these rate predictions are valid only for the extreme situation when $(k_{12} + k_{21}) \gg k_{23}$, namely, when the first equilibrium has been fully established before the start of the second step. When this requirement is not met, like in the experiments presented here, or there is no information about the rate in the equilibrium step, kinetic predictions without detailed analysis can easily result in unjustified conclusions.

There is an interesting parallel between a slow-fast mechanism and a mechanism containing a reversible step. Using the algebraic kinetic analysis method, it can be demonstrated that both of these physical mechanisms produce very similar second intermediate when analyzed using a unidirectional sequential scheme, namely, the second calculated sequential intermediate appears to be a mixture of the first and second intermediates of the physical mechanism. When analyzing real experimental data, the underlying slow-fast mechanism can therefore be mistakenly identified as a mechanism containing a reversible step. However, a quantitative kinetic analysis can distinguish between the two choices and identify the most probable underlying mechanism.

O_2 Concentration Dependence of the Reaction Rates. Measuring the dependence of observed rates on reactant concentration is traditionally considered to be a direct experimental approach for identifying which step corresponds to the bimolecular reaction in question. This technique works best for a mechanism involving irreversible steps well separated in time but less well for a mechanism with reversible steps or steps with closely spaced rates, as in our experiment. It is difficult to produce O_2 concentration higher than approximately 100 μM using the O_2 carrier, and at lower O_2 concentrations, we would expect the first two apparent rates to merge if the fastest step represents the O_2 binding. Alternatively, if the second fastest step is the O_2 binding, one would expect a very small accumulation of compound **A**. Despite these complications, we measured the kinetics at half the O_2 concentration (approximately 45 μM) used in our original experiment. We recorded the time-resolved absorption difference spectra in the 1 μs–10 ms time window for the ba_3-without-CO sample (Fig. S4). The inset shows the absorbance changes at 444 m, the absorbance maximum of the reduced heme a_3, at 90- and 45-μM O_2 concentrations. It is clear that the early kinetics are slower at the lower O_2 concentration; similar slowed-down kinetics are observed at other characteristic wavelengths. Both the reversible O_2 binding and the slow-fast mechanisms predict this type of kinetic response and therefore visual inspection of these traces is insufficient for solving the kinetic problem. However, by analyzing the time-resolved multiwavelength data using SVD and global exponential fitting, we were able to resolve four apparent lifetimes: 4.6 μs, 18 μs, 51 μs, and 0.93 ms. It is clear that the 9.3-μs lifetime observed at 90 μM O_2 is increased by a factor of two at the reduced O_2 concentration while the 4.8-μs lifetime is unaffected. This shows that the 9.3 μs lifetime indeed represents the O_2 binding step and that the binding is practically irreversible. The corresponding b-spectra were very similar to the ones observed at the higher O_2 concentration except the first one, which has a reduced amplitude and a higher level of noise; this is expected because of the small accumulation of compound **A**. The intermediate spectra calculated based on a traditional sequential scheme (Scheme 2) agree well with those obtained at higher O_2 concentration (approximately 90 μM), except that the spectrum of Int 2 (compound **A**) is further reduced in size (roughly half) (Fig. S5*a*). When the slow-fast mechanism (Scheme 5) was applied with appropriate rates, the calculated spectrum of compound **A** (Fig. S5*b*, green curve) matched the expected model spectrum (Fig. S5*b*, red curve) and the corresponding one obtained at 90-μM O_2 concentration within experimental uncertainty, providing further confirmation for the slow-fast mechanism (Fig. S5*b*).

$$\text{Int 1 } (\mathbf{R}) \underset{k_{21}}{\overset{k_{12}}{\rightleftarrows}} \text{Int 2 } (\mathbf{A}) \overset{k_{23}}{\rightarrow} \text{Int 3 } (\mathbf{P_I}) \overset{k_{34}}{\rightarrow} \text{Int 4 } (\mathbf{P_{II}}) \overset{k_{45}}{\rightarrow} \text{Int 5 } (\mathbf{O})$$

Scheme S1. The sequential scheme involving a reversible first step (O_2 binding) during the reaction of ba_3 with photoproduced O_2 in the absence of CO. Note that k_{12} is a pseudo-first-order rate constant: $k_{12} = k[O_2]$.

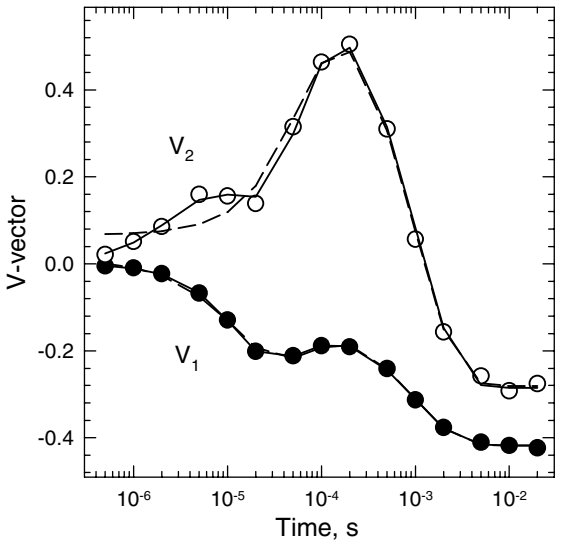

Fig. S1. The first two significant **v**-vectors, $\mathbf{v_1}$ (solid circles) and $\mathbf{v_2}$ (open circles) resulting from the SVD of the time-resolved data recorded during the reaction of reduced ba_3 with dioxygen in the absence of CO; the **v**-vectors describe the time evolution of the corresponding orthonormal basis spectra (**u**-spectra). The broken and solid lines represent the reproduced vectors of a three-exponential fit (broken lines; apparent lifetimes of 14 μs, 60 μs, and 1.0 ms) and a four-exponential fit (solid lines; apparent lifetimes of 4.8 μs, 9.3 μs, 55 μs, and 1.0 ms).

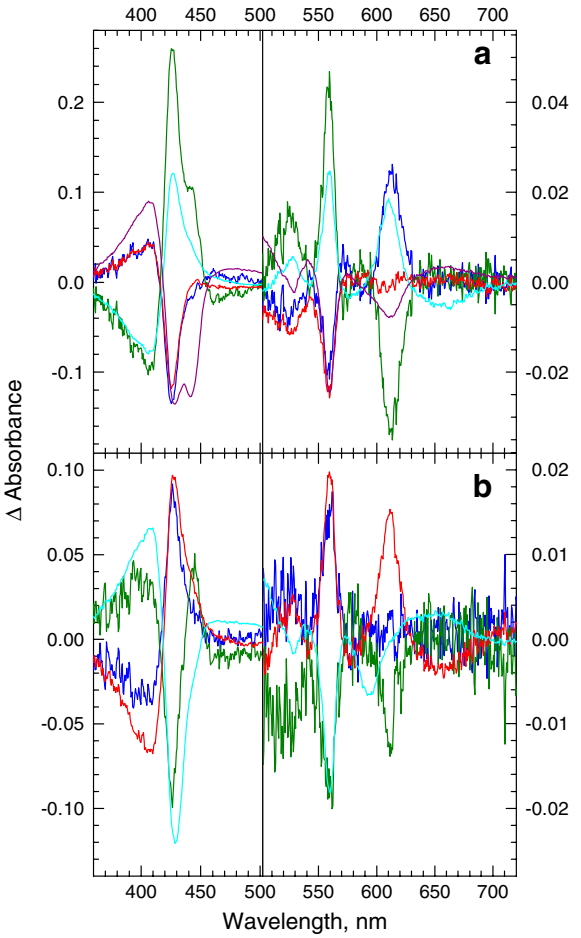

Fig. S2. (*A*) The spectral amplitudes (*b*-spectra) from a four-exponential fit to the time-resolved data recorded during the reaction of reduced ba_3 with dioxygen in the absence of CO: b_1 (blue, 4.8 μs), b_2 (green; 9.3 μs), b_3 (red, 55 μs), and b_4 (cyan, 1.0 ms). The nonzero time-independent b_o spectrum (magenta) represents the difference spectrum extrapolated to infinite time. (*B*) The spectral amplitudes (*b*-spectra) from a three-exponential fit to the time-resolved data recorded during the reaction of reduced ba_3 with dioxygen in the presence of CO: b_1 (blue, 59 μs), b_2 (green, 110 μs), and b_3 (red, 820 μs); b_0 (cyan) is the time-independent *b*-spectrum present at the end of the reaction.

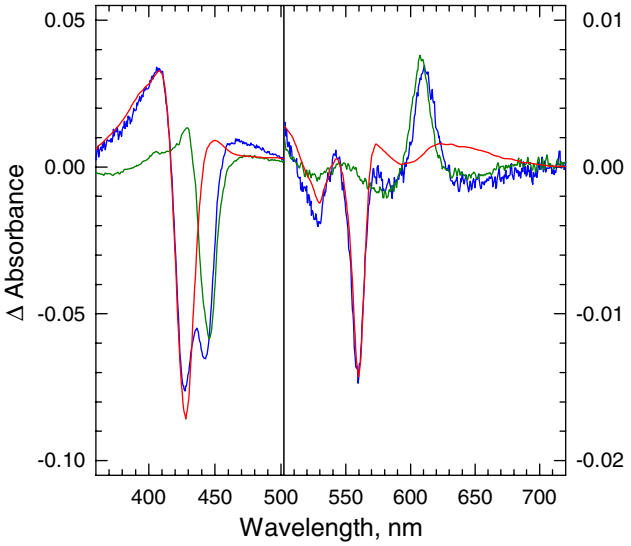

Fig. S3. The experimental and model spectra of intermediate 3 (P_I) during the reaction of ba_3-without-CO with dioxygen. The experimental spectrum (blue) was extracted from the time-resolved data in Fig. 1*A* based on Scheme 2. The experimental spectrum is modeled by the bovine heme a_3 **P** spectrum referenced versus reduced heme a_3 (green curve) and the oxidized-minus-reduced spectrum of heme *b* (red).

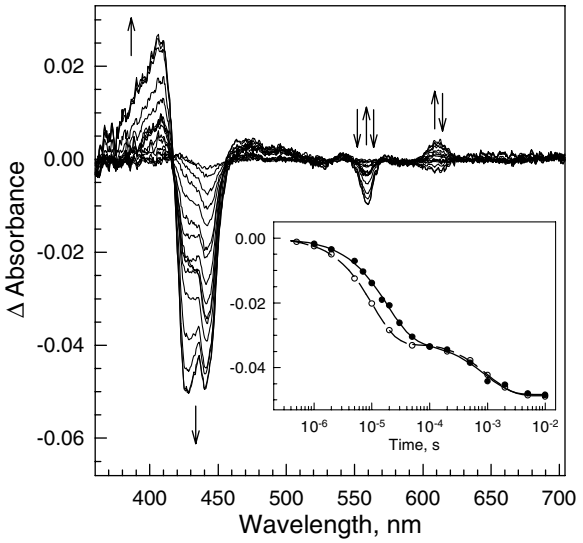

Fig. S4. Time-resolved optical absorption difference spectra (post- minus pre-photolysis) of the reduced ba_3 recorded in the absence of CO at 45 μM O_2 concentration. The spectra are those obtained after subtracting the spectral contribution of the O_2 complex, determined in a separate experiment. The spectra (SVD-filtered) were recorded at 16 delay times between 1 μs and 10 ms. The arrows (left to right) represent the direction of the absorbance change with time. Conditions: 0.1 M HEPES (pH 7.5), 0.1% DM; effective enzyme concentration: 1 μM; optical path, 0.5 cm. (*Inset*) A comparison of the transient absorbance changes at 444 nm at 90- and 45-μM O_2 concentrations (open and closed circles, respectively); the broken and solid lines represent the absorbance traces calculated on the basis of the global exponential fits.

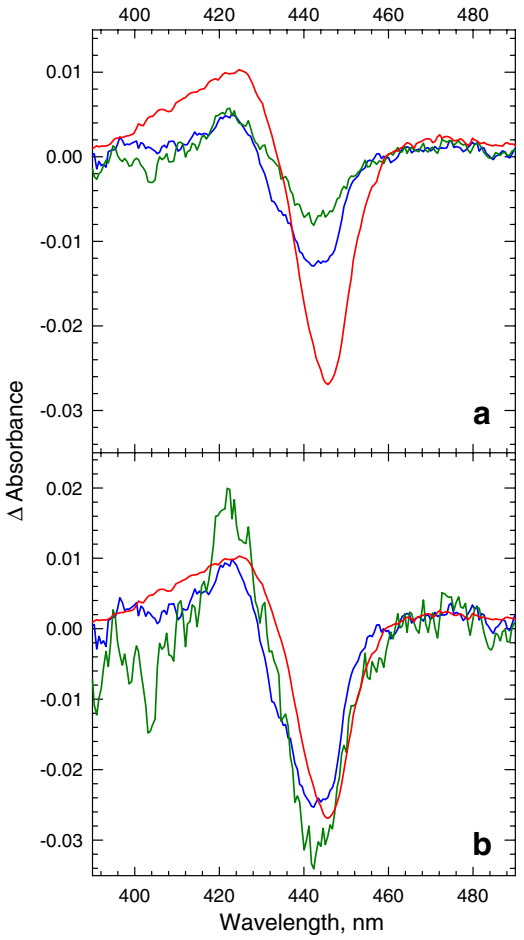

Fig. S5. The spectra of Int 2 for ba_3-without-CO at 90-μM O_2 (blue traces) and 45-μM O_2 (green traces) calculated using the traditional unidirectional fast-slow mechanism (*A*) and the slow-fast rate combination (*B*). The spectrum of compound **A** of the bovine aa_3 (CO flow-flash method) is the model spectrum (red curve).

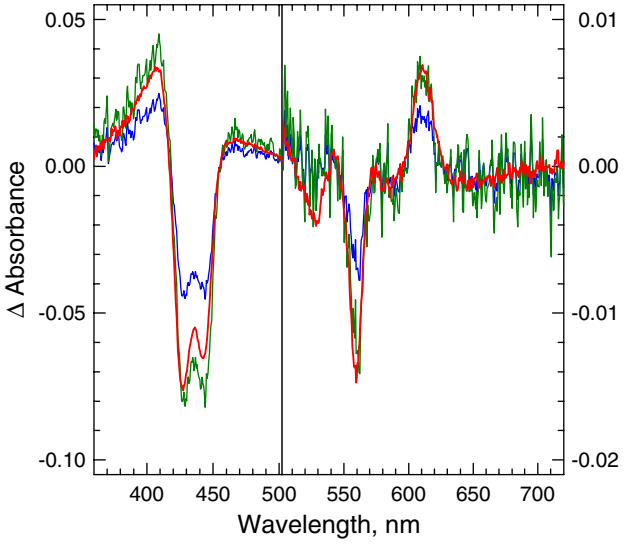

Fig. S6. (Blue) The spectrum of Int 2 for ba_3-with-CO using the fast-slow unidirectional sequential mechanism (Scheme 3). (Green) The spectrum of Int 2 for ba_3-with-CO using the slow-fast mechanism (Scheme 6). (Red) The model spectrum of $\mathbf{P_I}$ for ba_3-without-CO.